Advanced Controllers for Microelectromechanical Actuators

Robert N. Dean, Jr. John Y. Hung Bogdan M. Wilamowski
Electrical & Computer Engineering Department
200 Broun Hall
Auburn, AL 36849-5201
Phone: +1-334-844-1813, Fax: +1-334-844-1809
Email: rdean@eng.auburn.edu, j.y.hung@ieee.org, wilam@ieee.org

***Abstract*— We survey the recent methods for improving position control of electrostatic microelectromechanical (MEMS) actuators, and present recent new nonlinear approaches being studied in our electronic packaging and control systems laboratories. The new methods include a type of variable structure control (switching, but not sliding mode) and two methods for feedback linearizing control.**

I. Introduction

In addition to rather simple applications such as temperature or pressure measurement, MEMS technology has been identified for a number of advanced applications, including environmental MEMS sensors for engineering system monitoring, RF-MEMS, optical MEMS devices for beam steering, and micro-optic 'benches' for opto-electronics miniaturization. Many of these MEMS based systems rely on micromachined electrostatic actuators to provide translational and/or rotational motion to micro-members. A number of applications require multiple MEMS devices where each requires one or more electrostatic actuators . One example would be miniature MOEMS mirror array chips for adaptive optic systems, potentially useful for low-cost advanced optical systems. Each individual mirror pixel (pixilated mirror array) or push-rod (continuous membrane mirror chip) is attached to a MEMS electrostatic actuator. A method that would increase the useful throw range of the actuator by a factor of almost three, as well as reduce the required drive voltage and packaged device volume, would result in smaller, lower-cost and higher performance end-use systems. Micromachined RF devices typically use one or more electrostatic actuators to realize RF elements such as switches and variable capacitors. Likewise they would benefit by the use of enhanced actuators with greatly increased throw range without sacrificing low-voltage operation and miniature size. Other micromachined optical devices also utilize MEMS electrostatic actuators, such as MEMS based photonic bandgap filters, and could benefit from enhanced actuator throw range.

II. MEMS Models and Analysis

Mechanical motion dynamics of MEMS devices are described by second-order models of the form

$$M\ddot{x} + k(x) = F_e \tag{1}$$

Here

x	actuator position
M	inertia
$k(x)$	elastic force due to mechanical compliance
F_e	force of electrostatic origin.

The force of electrostatic origin is typically a nonlinear function of actuator voltage v and actuator position x. Electrostatic force can be derived from stored energy models, which in turn can be computed from the actuator capacitance. When a voltage v is applied, the resulting electrostatic force pulls the movable part toward the stationary plate, until balanced by the spring force (compliance) of the movable structure. If the applied voltage is increased slowly, so that the inertial and damping forces can be accurately approximated as zero, a force balance between mechanical compliance and electrostatic force results. The nature of the nonlinear electrostatic force is such that two equilibrium points exist in the force balance model. One of the equilibrium points is unstable, and the other is stable. As applied voltage increases, the two equilibrium points move closer together. At the so-called "pull-in" voltage, the two equilibrium points merge into one unstable equilibrium point. Beyond the pull-in voltage, the actuator parts snap together.

Two common types of actuators are discussed next.

A. Parallel Plate Actuator

The structure of a simple MEMS parallel plate actuator (PPA) is illustrated in Fig. 1(a). A silicon-on-insulator wafer with a doped (conductive) handle layer is used to fabricate the simple PPA. The 10 μm thick Si device layer is used to set the rest gap x_o between the two electrodes (parallel actuator plates). The Si handle layer comprises the stationary plate, and is electrically connected to form the backside of the device. A 1 μm thick aluminum layer is vapor deposited on top of a thin nonconductive silicon dioxide on the Si device layer, which is patterned to realize the movable actuator plate, a trampoline configured spring-mass-damper structure with eight springs. Although a simple implementation, this type of PPA has been used to realize pixilated micro-mirror arrays for research in adaptive optics systems [1]. A photograph of a silicon PPA's movable electrode for use in advanced packaging of a MEMS gyroscope die [2] is shown in Fig. 1(b).

Consider two parallel plates separated by a free space

0-7803-9484-4/05/$20.00 ©2005 IEEE

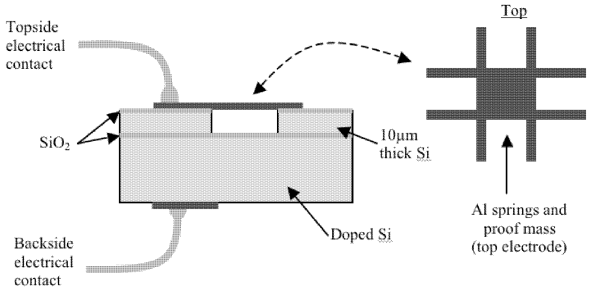

(a) Illustration of PPA structure

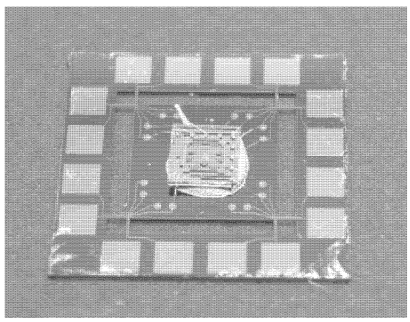

(b) A Si PPA movable electrode for use in advanced packaging of MEMS gyroscope die [2]

Fig. 1. MEMS parallel plate actuator (PPA)

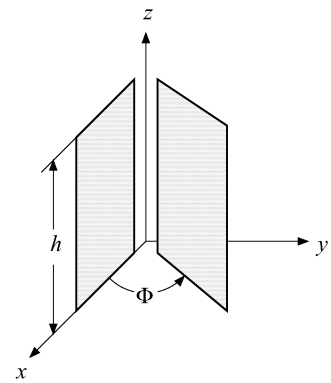

(a) "Cake slice" capacitor model.

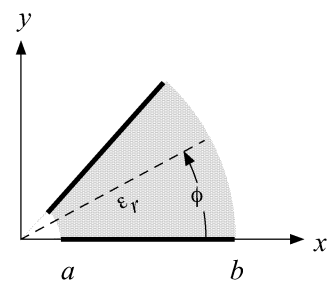

(b) Cross-section of the capacitor model.

Fig. 2. Model of capacitor having non-parallel plates.

distance x. The permittivity of free space is $\epsilon_o = 8.8542 \times 10^{-12}$ F/m or $C^2/N/m^2$. Given the plate area A, the capacitance C of the system is given by

$$C = \frac{\epsilon_o A}{x} \tag{2}$$

Observe that capacitance is proportional to plate area A, and inversely proportional to distance x. The stored charge q is given by

$$\begin{aligned} q &= Cv \\ &= \epsilon_o A \frac{v}{x} \end{aligned} \tag{3}$$

where v is the voltage across the plates. Energy stored in the system is given by

$$\begin{aligned} W &= \frac{1}{2} q v \\ &= \frac{\epsilon_o A}{2} \left(\frac{v^2}{x} \right) \end{aligned} \tag{4}$$

Electrostatic force is derived using the virtual displacement principle:

$$\begin{aligned} F_e &= \frac{\partial W}{\partial x} \\ &= -\frac{\epsilon_o A}{2} \left(\frac{v}{x} \right)^2 \end{aligned} \tag{5}$$

There exists a maximum achievable displacement before the pull-in voltage is reached. This distance is equal to $x_o/3$, and is independent of the spring constant k. Therefore, for open loop application where a voltage source is directly connected to the parallel plate electrostatic actuator, the stable range of motion is $0 \leq x < x_o/3$.

B. Tilt Axis Actuator

The tilt-axis actuator can be modeled as a capacitor having non-parallel plates, which in turn can be modeled as a "cake slice". In cylindrical coordinates (r, ϕ, z), the model appears as shown in Fig. 2(a). The angle between plates is Φ, and the height of the capacitor is denoted by h. The cross-sectional view (Fig. 2(b)) shows a capacitor plate along the x-axis between the coordinates a and b. The second (upper) plate is identical to the first (lower) plate, but is rotated about the z-axis. The positive sign convention for angle ϕ is shown in Fig. 2(b). The interior of the capacitor is indicated by the shaded region, and the dielectric's relative permittivity is denoted by ϵ_r. Free-space permittivity is denoted by ϵ_o.

1) The General Approach: The general approach for deriving the device capacitance is as follows [3]:

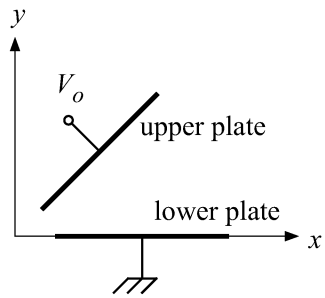

Fig. 3. Applying voltage V_o to the capacitor.

1) Place voltage V_o on the upper plate and ground the lower plate.
2) Positive and negative charges are distributed across the plates, and there is no charge in the region between the plates. Therefore, the Laplacian relation is true, and can be used to solve for the voltage V in the interior of the capacitor:

$$\nabla^2 V = 0$$

3) From the voltage V, compute the electric field (negative gradient of the voltage)

$$\overrightarrow{E} = -\nabla V$$

4) In the dielectric, electric displacement $\overrightarrow{D}$ is related to the electric field $\overrightarrow{E}$ by

$$\overrightarrow{D} = \epsilon_r \epsilon_o \overrightarrow{E}$$

where ϵ_r and ϵ_o are the dielectric relative permittivity and free-space permittivity, respectively. At the conductor-dielectric boundary, the normal component of $\overrightarrow{D}$ must have magnitude equal to the charge density ρ_s. At the upper plate,

$$\rho_s = -D$$

The negative sign arises because the orientation of the displacement vector $\overrightarrow{D}$ is opposite to the positive sign convention for the angle ϕ.
5) The total charge can be computed from the surface charge density by using the surface integral

$$Q = \int \rho_s dS$$

where the incremental area is given by

$$dS = drdz$$

6) Finally, the capacitance is given by

$$C = \frac{Q}{V_o}$$

2) Step-by-Step Details:

1) Voltage V_o is applied as illustrated in Fig. 3.
2) In cylindrical coordinates, the Laplacian $\nabla^2 V$ is computed as

$$\frac{1}{r}\frac{\partial}{\partial r}\left(r\frac{\partial V}{\partial r}\right) + \frac{1}{r^2}\frac{\partial^2 V}{\partial \phi^2} + \frac{\partial^2 V}{\partial z^2}$$

In this problem, angle ϕ is the only variable, so only the second term is non-zero. Therefore

$$\frac{1}{r^2}\frac{\partial^2 V}{\partial \phi^2} = 0$$

A solution is given by

$$V = k_1\phi + k_2$$

where k_1, k_2 are constants that satisfy two boundary conditions:

a) Voltage on the lower plate equals zero (ground)

$$k_1(0) + k_2 = 0$$

b) Voltage at the upper plate (angle = Φ) equals V_o

$$k_1\Phi + k_2 = V_o$$

Solving for k_1, k_2 yields

$$k_1 = \frac{V_o}{\Phi}, \qquad k_2 = 0$$

Therefore, the voltage in the region between the two plates is given by

$$V = \frac{V_o}{\Phi}\phi \tag{6}$$

The interior voltage is proportional to the angle ϕ.
3) Electric field is the negative gradient of the voltage V. In cylindrical coordinates, the gradient operator is defined as

$$\nabla = \frac{\partial}{\partial r}\hat{r} + \frac{1}{r}\frac{\partial}{\partial \phi}\hat{\phi} + \frac{\partial}{\partial z}\hat{z}$$

In this problem, only the $\hat{\phi}$ component is non-zero. Substituting (6) into the gradient expression yields

$$\begin{aligned}\overrightarrow{E} &= -\nabla V \\ &= -\frac{1}{r}\frac{\partial V}{\partial \phi}\hat{\phi} \\ &= -\frac{V_o}{r\Phi}\hat{\phi}\end{aligned} \tag{7}$$

4) From electric field (7) the displacement is given by

$$\overrightarrow{D} = -\frac{\epsilon_r \epsilon_o V_o}{r\Phi}\hat{\phi}$$

Therefore, the surface charge density is

$$\rho_s = \frac{\epsilon_r \epsilon_o V_o}{\Phi}\frac{1}{r} \tag{8}$$

A sketch of the electric field lines (7) and charge distribution (8) is shown in Fig. 4. Examples of the electric displacement (vector) are also shown at the upper and lower plates.

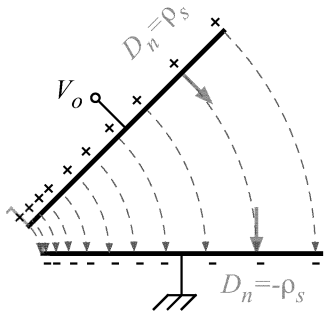

Fig. 4. Electric field lines and charge distribution.

5) Having found the surface charge density (8), the total charge is calculated:

$$\begin{aligned} Q &= \int \rho_s dS \\ &= \frac{\epsilon_r \epsilon_o V_o}{\Phi} \int_a^b \frac{1}{r} dr \int_0^h dz \\ &= \frac{\epsilon_r \epsilon_o V_o h}{\Phi} \ln\left(\frac{b}{a}\right) \end{aligned} \tag{9}$$

6) Capacitance of the "cake slice" model is finally computed as:

$$\begin{aligned} C &= \frac{Q}{V_o} \\ &= \frac{\epsilon_r \epsilon_o h}{\Phi} \ln\left(\frac{b}{a}\right) \end{aligned} \tag{10}$$

From the capacitance model, the electrostatic force F_e can be computed in a manner identical to that used for the parallel plate actuator (Sec. II-A).

III. Survey of Control Methods

Dynamic models of electrostatic actuators are dual to those of electromagnetic suspension systems (Hung [4]). The form of equations are similar and both classes of actuator share similar force nonlinearities. As such, there are many similarities among the control techniques that can be employed. Beyond the control theory, however, are physical implementation issues. The physical scale of MEMS actuators is such that many advanced control techniques have not been implemented or explored until recently.

Several methods for controlling electrostatic MEMS platforms exist. A simple, open loop method of increasing the controllable range of motion of a PPA, as described by Bao [5], is to design the actuator to have a rest distance that is three times the required range of motion. In this way, the actuator never leaves the open loop stable operating range, $0 \leq x < x_o/3$. A second but equivalent technique to realize this effect is to put an appropriately sized capacitor in series with the PPA, which makes the capacitor-PPA combination appear as a PPA with a rest gap three times larger than it actually has. A drawback of these techniques is the requirement of a much larger drive voltage.

Chen et al. [6] employ a modest linear gain schedule to improve motion in a MEMS optical switch application. Their method has the advantage of being simple to design and implement, but does not capture all of the effects of the actuator nonlinearity. Actuator nonlinearity can lead to significant performance problems, including chaotic oscillations (Liu et al [7]).

The extreme nonlinearity of the electrostatic actuator can be partially addressed by the physical layout and design of the actuator. For example, Rosa et al [8] describe an external, tapered electrode to compensate for the nonlinear relationships between force, voltage, and gap distance. Chiou and Lin [9] use multiple electrodes to cover the operating range by several smaller motions.

Novel control approaches include the use of charge control (Seeger and Boser [10]). Using charge control, the extreme nonlinearity of force with respect to voltage and gap distance is largely avoided. A charge amplifier is required, however, and the approach does have some sensitivity to parasitic capacitance. Seeger and Boser have extended the application of the charge amplifier to a feedback configuration that produces the effect of negative capacitance [11], which also improves dynamic stability.

Chu and Pister [12] simulate a nonlinear control law that employs a square-root characteristic to compensate for the nonlinear relationship of force vs (voltage, distance). That control is straightforward to derive from the 2nd-order mechanical dynamics model and can be expressed in analytical form, but implementation was not easy to perform or test with the technologies of the early 1990s.

IV. Recent New Approaches

Advances in nonlinear control theory and analog electronic circuit design tools now make is possible to address the nonlinear MEMS actuator control problems. Several advances being studied at Auburn University are described here.

A. Variable Structure Control

Dean et al [2] have been investigating the application of electrostatic MEMS as vibration isolation platforms for MEMS gyroscopes. The MEMS actuator platform has inherently light damping that can be greatly improved by nonlinear control. The velocity of the MEMS platform is measured, and the actuator voltage is applied only when the velocity is increasing (gap is increasing). Dean's "skyhook" control method [2] can be explained using variable structure control theory. The natural zero-input response of the MEMS platform is lightly damped; the response can be described by circles in the phase portrait (Fig. 5(a)). If a constant voltage is applied, then the actuator platform deflects to a new steady-state position a, but the damping is unchanged. Under constant voltage input, the phase portrait is described by circles that have been shifted by a distance a (Fig. 5(b)). The variable structure control proposed by Dean applies the control voltage only when the actuator gap is increasing. The resulting response in the phase plane is the composite of the two lightly damped responses,

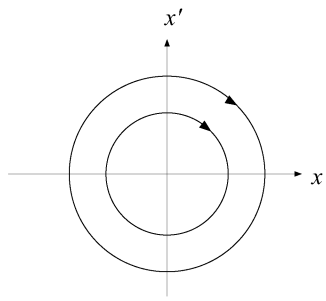

(a) Zero-input response

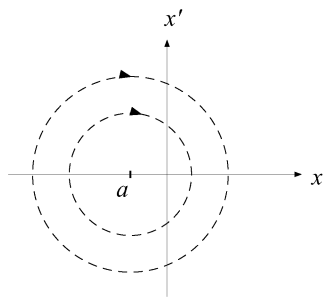

(b) Constant-input response

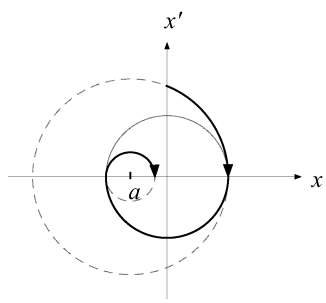

(c) Variable structure response

Fig. 5. Explanation of "skyhook" control

as illustrated by the bold curve in Fig. 5(c). Note that this is not a sliding mode control, but a classical variable structure system.

B. Series Capacitance with Added Bias

Recall from the series capacitor control technique described above that a capacitor can be placed in series with a MEMS PPA actuator - the capacitance value is such that the series capacitor-PPA combination electrically appears as a PPA with a rest gap three times larger than the actual rest gap. Therefore the total range of motion of the PPA is within the stability range of the apparent PPA. The major drawback of this technique is the high required input voltage across the series capacitor-PPA pair. Note that the PPA actuator drive voltage v is actually much smaller than the input voltage v_c that appears across the capacitor-actuator pair. Therefore, more advanced structures with extra biasing of the node between the capacitor and actuator can be explored. Two different controllers could be used, one for dc bias control, and the other for dynamic control of the actuator.

C. Series Capacitance Emulation

The effect of the series capacitor can also be achieved by a nonlinear control that emulates the series capacitance effect. Circuit analysis reveals a nonlinear mapping between the input control voltage v_c and the actuator drive voltage v. For the series capacitor utilized with a parallel plate actuator, the nonlinear mapping function is given by:

$$\frac{v}{v_c} = \frac{x_o - x}{3x_o - x} \tag{11}$$

where x_o is the PPA rest gap distance and x is the displacement of the movable electrode toward the fixed electrode. The nonlinear mapping (11) emulates the effect of a series capacitor, and increases the static range of the actuator beyond the natural pull-in limit. The nonlinear mapping directly produces the proper lower voltage across the PPA without incurring the high voltage penalty of producing the voltage across a series capacitor.

Although the nonlinear mapping function mathematically emulates the result of adding a capacitor in series with the PPA, one is not restricted to that function. Many nonlinear mapping functions can be utilized to transform the PPA electrostatic force relation to a linear behavior.

D. State Linearization

Dynamic linearization of MEMS electrostatic actuators is a challenge due to the square-law nature of the electrostatic force, and the limits of the restoring mechanical compliance forces. The analogy is that of the well-known magnetic levitation with a single electromagnet working against gravity. At Auburn University, we are studying methods to achieve partial linearization across wide dynamic range by using a hybrid combination of variable structure control for damping (Sec. IV-A) and static linearization of the electrostatic force (Sec. IV-C).

V. Analog Electronic Implementation

For nonlinear control to be practical in MEMS actuator applications, we are investigating application specific VLSI circuits that can be developed to implement the required nonlinear functions [13]. For example Fig. 6 shows the circuit diagram which implements a cosine function. Fig. 7 shows a signal divider circuit that could be used to implement the division operation needed for the series capacitor emulation nonlinear mapping (11). There are many possible circuits for creating various nonlinear functions by using the nonlinear characteristics of semiconductor devices. Such circuits are relatively simple and fast; their main disadvantage is that the obtained functions may not be highly accurate, and may strongly depend on element tolerances. However, in many

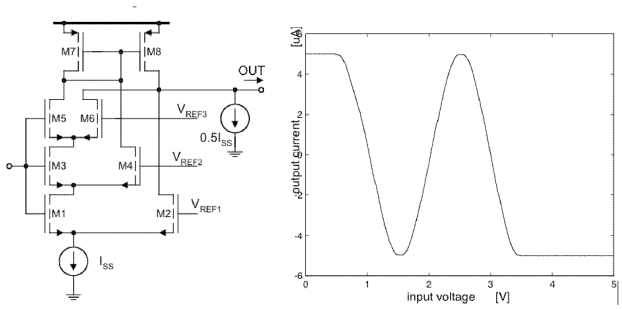

(a) circuit (b) output response

Fig. 6. VLSI implementation of cosine nonlinear function [13]

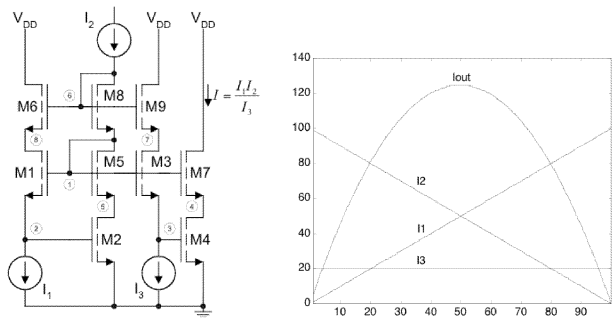

(a) circuit (b) output response

Fig. 7. VLSI implementation of a signal divider [13]

control applications this is not a serious issue since nonlinear functions are often used to "linearize" dynamics so that robust linear control methods can be applied. To be effective this linearization need not to be perfect, so long as major nonlinearities are eliminated.

VI. Conclusion

We have presented models for basic MEMS parallel plate and tilt actuators, analysis, and a survey of recent control methods for MEMS electrostatic actuator systems. The survey also summarizes our ongoing studies to implement nonlinear control methods for MEMS, using analog VLSI circuits. The goal is to improve or enhance the closed loop characteristics, including increasing the stable range of motion beyond the open loop pull-in point and/or reducing the required actuator drive voltage.

References

[1] R. L. Clark, J. R. Karpinisky, J. A. Hammer, R. B. Anderson, R. L. Lindsey, D. M. Brown, and P. H. Merritt, "Micro-opto-electromechanical (MOEM) adaptive optic system," in *Proceedings of SPIE: Miniaturized Systems with Micro-optics and Micromechanics II*, vol. 3008, 1997, pp. 12–24.

[2] R. N. Dean, G. Flowers, N. Sanders, K. MacAllister, R. Horvath, A. S. Hodel, W. Johnson, M. Kranz, and M. Whitley, "Damping control of micromachined lowpass mechanical vibration isolation filters using electrostatic actuation with electronic signal processing," in *Proceedings of SPIE International Symposia on Smart Structures & Materials*, San Diego, CA, March 2005.

[3] S. M. Wentworth, *Fundamentals of Electromagnetics with Engineering Applications*. John Wiley & Sons, 2005.

[4] J. Y. Hung, N. G. Albritton, and F. Xia, "Nonlinear control of a magnetic bearing system," *Mechatronics (Pergamon Press)*, vol. 13, no. 6, pp. 621–637, July 2003.

[5] M.-H. Bao, *Handbook of Sensors and Actuators*. New York: Elsevier Science, 2000, vol. 8.

[6] J. Chen, W. Weingartner, A. Azarov, and R. C. Giles, "Tilt-angle stabilization of electrostatically actuated micromechanical mirrors beyond the pull-in point," *Journal of Microelectromechanical Systems*, vol. 13, no. 6, pp. 988–997, December 2004.

[7] S. Liu, A. Davidson, and Q. Lin, "Simulation studies on nonlinear dynamics and chaos in a MEMS cantilever control system," *Journal of Micromechanics and Microengineering*, vol. 14, pp. 1064–1073, June 2004.

[8] M. A. Rosa, D. D. Bruyker, A. R. Völkel, E. Peters, and J. Dunec, "A novel external electrode configuration for the electrostatic actuation of MEMS based devices," *Journal of Micromechanics and Microengineering*, vol. 14, pp. 446–451, January 2004.

[9] J.-C. Chiou and Y.-C. Lin, "A multiple electrostatic electrodes torsion micromirror device with linear stepping angle effect," *Journal of Microelectromechanical Systems*, vol. 12, no. 6, pp. 913–920, December 2003.

[10] J. I. Seeger and B. E. Boser, "Charge control of parallel-plate, electrostatic actuator and the tip-in instability," *Journal of Microelectromechanical Systems*, vol. 12, no. 5, pp. 656–671, October 2003.

[11] ——, "Negative capacitance for control of gap-closing electrostatic actuators," in *12th International Conference on Solid-State Sensors, Actuators and Microsystems*, Boston, MA, June 2003, pp. 484–487.

[12] P. B. Chu and K. S. J. Pister, "Analysis of closed-loop control of parallel-plate electrostatic microgrippers," in *Proceedings of 1994 International Conference on Robotics and Automation*, San Diego, CA, May 1994, pp. 820–825.

[13] B. M. Wilamowski, J. Y. Hung, and R. Gottiparthy, "Digitally tuned analog vlsi controllers," in *2005 IEEE International Symposium on Industrial Electronics*, Dubrovnik, CROATIA, June 2005.